

MITIGATING LONG-TAIL BIAS VIA PROMPT-CONTROLLED DIFFUSION AUGMENTATION

Buddhi Wijenayake¹, Nichula Wasalathilake¹, Roshan Godaliyadda¹,
Vijitha Herath¹, Parakrama Ekanayake¹, Vishal M. Patel²

¹ University of Peradeniya, Peradeniya, Sri Lanka

² Johns Hopkins University, Baltimore, Maryland, USA

{e19445,e20425,roshang,vijitha,mpbe}@eng.pdn.ac.lk, vpatel36@jhu.edu

Abstract—Semantic segmentation of high-resolution remote-sensing imagery is critical for urban mapping and land-cover monitoring, yet training data typically exhibits severe long-tailed pixel imbalance. In LoveDA, this challenge is compounded by an explicit Urban/Rural split with distinct appearance and inconsistent class-frequency statistics across domains. We present a prompt-controlled diffusion augmentation framework that synthesizes paired label-image samples with explicit control of both domain and semantic composition. Stage A uses a domain-aware, masked ratio-conditioned discrete diffusion model to generate layouts that satisfy user-specified class-ratio targets while respecting learned co-occurrence structure. Stage B translates layouts into photorealistic, domain-consistent images using Stable Diffusion with ControlNet guidance. Mixing the resulting ratio and domain controlled synthetic pairs with real data yields consistent improvements across multiple segmentation backbones, with gains concentrated on minority classes and improved Urban and Rural generalization, demonstrating controllable augmentation as a practical mechanism to mitigate long-tail bias in remote-sensing segmentation. Source codes, pretrained Models and synthetic datasets are available at [Github](#)

Index Terms—Class imbalance, data augmentation, diffusion models, remote sensing, semantic segmentation.

I. INTRODUCTION

Semantic segmentation of high-resolution remote sensing imagery supports key geospatial applications such as urban mapping, land-cover monitoring, and environmental assessment [1, 2]. However, performance in realistic settings is often limited by severe pixel-level class imbalance where a few dominant categories occupy most pixels, while minority classes appear sparsely, creating a long-tailed training signal that biases learning toward frequent classes and degrades rare-class recognition.

This challenge is amplified in LoveDA [3], which is explicitly organized into Urban and Rural domains with distinct scene structure, appearance, and inconsistent class distributions across domains (Fig. 1(a)). Several semantically important categories occupy only a small fraction of pixels, and the tail classes differ between Urban and Rural splits [3]. As a result, models must jointly address within-domain long-tail imbalance and cross-domain shift, an interaction that standard supervised training often struggles to resolve [3].

Common remedies include class re-weighting [4], focal-

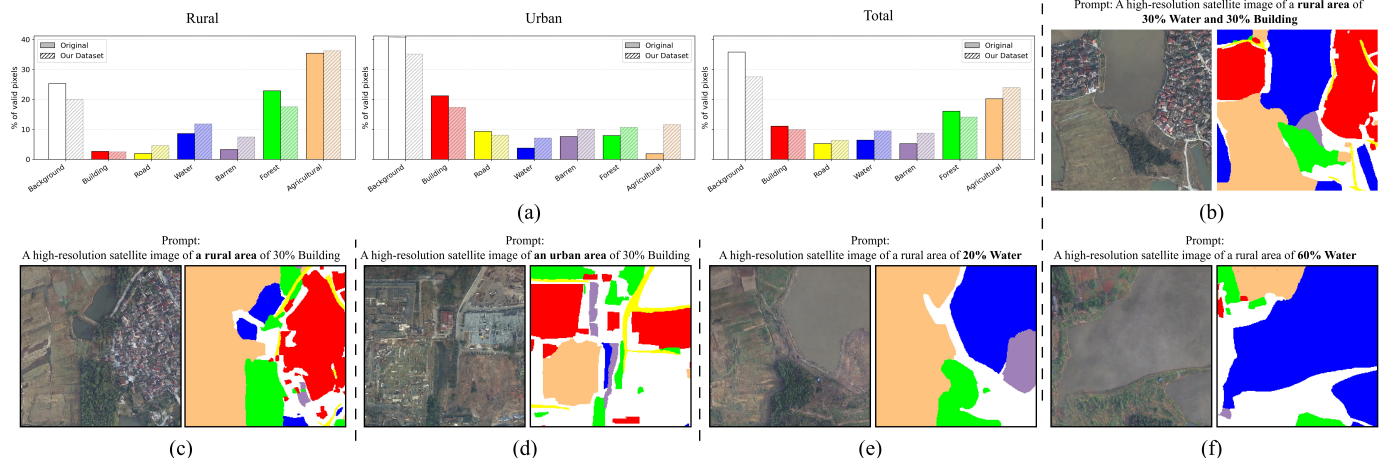


Fig. 1: Dataset balancing and prompt-controllable synthesis on LoveDA. (a) Pixel-frequency distributions for Rural, Urban, and the combined training set, comparing the original data (solid) against our augmented dataset (hatched). (b–f) Representative synthesized image-label pairs generated under explicit domain (Urban/Rural) and class-ratio constraints, illustrating controllable diffusion for both domain-consistent appearance and targeted semantic proportions.

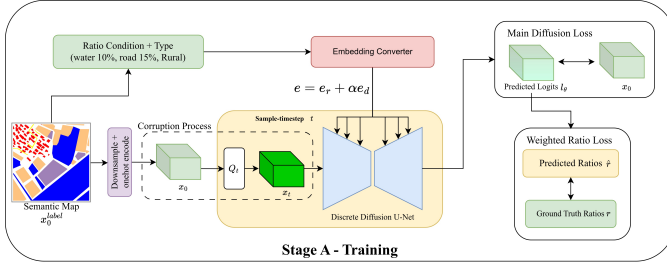


Fig. 2: Stage A: domain and ratio conditioned discrete diffusion (D3PM) for semantic layout generation. A U-Net denoiser predicts categorical logits from a noisy label map conditioned on a masked class-ratio target and Urban/Rural domain embedding.

style objectives [5], online hard example mining [6], resampling, and geometric/photometric augmentation [7]. While these strategies can stabilize optimization, they largely preserve the underlying pixel-frequency statistics and cannot reliably increase exposure to rare, spatially localized, context-dependent classes. Moreover, LoveDA’s domain-dependent imbalance makes naive re-weighting prone to domain-specific overfitting or head-class gains without consistent tail improvements across both splits [3].

Generative augmentation offers a complementary direction by synthesizing additional labeled data rather than only reshaping the loss. Diffusion models provide strong fidelity and diversity [8, 9], and recent Earth-observation work demonstrates diffusion-based satellite image generation and layout-conditioned synthesis [10, 11]. However, for long-tailed segmentation, realism alone is insufficient, and controllability is essential [12]. If a generator primarily matches the empirical training distribution, rare classes remain rare, and domain gaps may be reinforced [13–15].

In this work, we propose a prompt-controlled generative augmentation framework for LoveDA that explicitly conditions generation on domain (Urban/Rural) and partial class-ratio targets, enabling targeted synthesis that increases minority-class pixel exposure while preserving domain-consistent remote-sensing realism.

II. METHODOLOGY

The proposed architecture is a two-stage, domain-aware generative augmentation pipeline that synthesizes paired label-image samples with controllable semantic composition. In the first Stage (Stage A), a ratio and domain-conditioned discrete diffusion model (D3PM) [16] generates semantic layouts that match desired class-ratio targets within a specified domain. In the second stage (Stage B), a fine-tuned Stable Diffusion network translates these layouts into photorealistic remote-sensing images while preserving spatial structure and domain appearance. The resulting synthetic corpus is mixed with the real training set using a controlled sampling protocol to train the state-of-the-art segmentation models. Subsequent sections present each contribution in detail.

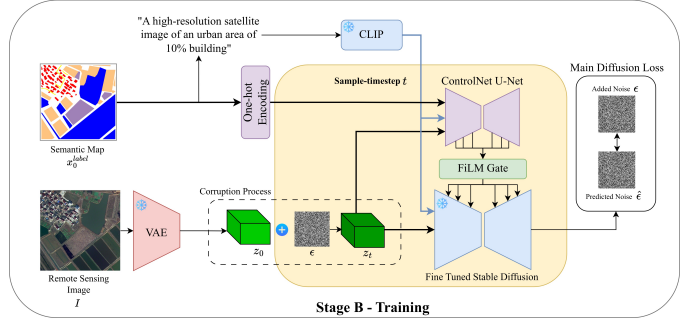


Fig. 3: Stage B: layout-guided latent diffusion for image synthesis. A Stable Diffusion U-Net is guided by ControlNet features from the layout, with FiLM-gated residual injection and a domain/ratio prompt for domain-consistent appearance.

A. Stage A: Ratio and Domain conditioned Discrete Layout Diffusion

Diffusion models define a forward noising process and learn a reverse denoising process to generate samples. While standard DDPMs operate in continuous spaces, Discrete Denoising Diffusion Probabilistic Models (D3PMs) extend this framework to categorical variables, making them well-suited for discrete structures such as semantic label maps [16].

As seen in figure 2, given a semantic map $x_0^{\text{label}} \in \{1, \dots, K\}^{H_e \times W_e}$ with K land-cover classes, we define its class-ratio vector as,

$$r(x_0^{\text{label}})_k = \frac{1}{|\Omega|} \sum_{(i,j) \in \Omega} \mathbb{1}[x_0^{\text{label}}(i,j) = k], \quad (1)$$

with $\sum_{k=1}^K r_k = 1$,

where Ω excludes ignored pixels. The semantic map will be downsampled and one-hot encoded to form $x_0 \in K \times 256 \times 256$.

a) *Forward corruption*: Stage A uses a D3PM forward Markov chain [16] given by,

$$q(x_{1:T} | x_0) = \prod_{t=1}^T q(x_t | x_{t-1}), \quad (2)$$

which is parameterized by a categorical transition matrix $Q_t \in \mathbb{R}^{K \times K}$. The scheduler samples the corrupted one-hot layout $x_t \sim q(x_t | x_0, t)$ [16].

b) *Conditioning*: We condition the denoiser on (i) a ratio target and (ii) a domain label $d \in \{\text{Urban}, \text{Rural}\}$. To support partial control, we randomly mask ratio constraints during training using $m \in \{0, 1\}^K$, where $m_k = 1$ indicates that class k is constrained. Inside the embedding converter shown in figure 2, a lightweight ratio projector maps the masked ratio input to a conditioning vector $e_r \in \mathbb{R}^{d_e}$ aligned with the diffusion time-embedding dimension. A learnable domain embedding $e_d \in \mathbb{R}^{d_e}$ is added to obtain the final conditioning embedding as, $e = e_r + \alpha e_d$ where α is a learnable scalar controlling the domain contribution.

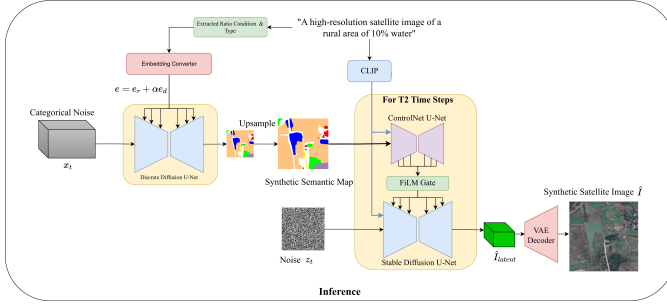


Fig. 4: Prompt-controlled inference pipeline. The prompt is parsed into domain and ratio targets, a layout is sampled with Stage A, and a photorealistic image is generated with Stage B using the sampled layout as spatial guidance.

c) *Reverse model*: A UNet denoiser f_θ takes the corrupted one-hot layout x_t , timestep t , and conditioning e , and outputs per-pixel class logits as,

$$\ell_\theta(x_t, t, e) = f_\theta(x_t, t; e) \in \mathbb{R}^{K \times H_t \times W_t}. \quad (3)$$

d) *Training objective*: Given logits ℓ_θ , we compute per-pixel class probabilities $p_\theta = \text{softmax}(\ell_\theta)$ and estimate the global class-ratio vector \hat{r}_k by averaging these probabilities over valid layout pixels similar to equation 1.

We then apply a two-weight ratio-matching loss that prioritizes constrained classes while softly regularizing unconstrained ones, which can be given as,

$$\mathcal{L}_{\text{ratio}} = \|m \odot (\hat{r} - r)\|_2^2 + 0.1 \|(1 - m) \odot (\hat{r} - r)\|_2^2. \quad (4)$$

The first term enforces the requested ratios, while the 0.1-weighted term encourages the model to complete the remaining composition using learned co-occurrence statistics rather than arbitrary allocation.

Following [16], we train the discrete diffusion model by minimizing the negative variational lower bound \mathcal{L}_{VLB} with an auxiliary denoising cross-entropy term \mathcal{L}_{CE} for stabilization, and add the masked ratio constraint to obtain the stage A loss function,

$$\mathcal{L}_A = \mathcal{L}_{\text{VLB}} + 0.5 \mathcal{L}_{\text{CE}} + \mathcal{L}_{\text{ratio}}. \quad (5)$$

B. Stage B: Layout-guided Image Synthesis with Ratio and Domain-aware ControlNet

As seen in figure 3, Stage B synthesizes a photorealistic remote-sensing image conditioned on (i) a semantic layout, and (ii) a domain-aware prompt. We build on latent diffusion models (LDMs) [9] and ControlNet [17], and use FiLM gating [18] to modulate ControlNet residual features.

a) *Latent diffusion*: Given an RGB remote-sensing image $I \in \mathbb{R}^{3 \times H \times W}$, a VAE encoder maps it to a latent representation $z_0 \in \mathbb{R}^{4 \times \frac{H}{8} \times \frac{W}{8}}$. A noise scheduler corrupts this latent as,

$$z_t = \alpha_t z_0 + \sigma_t \epsilon, \quad (6)$$

with $\epsilon \sim \mathcal{N}(0, I)$, $t \sim \mathcal{U}\{0, \dots, T-1\}$,

where (α_t, σ_t) follow the diffusion schedule [9]. The denoising model predicts the injected noise ϵ from (z_t, t) under multi-source conditioning.

b) *Conditioning signals*: A domain prompt (e.g., “a high-resolution satellite image of an urban area of 10% water” or “a high-resolution satellite image of a rural area of 30% building, 5% agriculture and 3% forest”) is encoded by a CLIP text encoder [19] to obtain token embeddings c_{text} . These embeddings condition both the ControlNet U-Net and the fine-tuned Stable Diffusion U-Net via cross-attention [9].

The semantic map x_0^{label} is converted into a K -channel one-hot tensor and fed to ControlNet as the conditioning input.

c) *Gated ControlNet residual injection*: Motivated by prior results showing that feature-wise affine modulation preserves semantic-layout conditioning in image synthesis [20], we adapt a ControlNet that takes the noisy latent, timestep, text embeddings, and one-hot layout conditioning, and outputs multi-scale residual features as,

$$\{\Delta^{(b)}\}, \Delta^{(\text{mid})} = \text{ControlNet}(z_t, t, c_{\text{text}}, x_0), \quad (7)$$

where $\Delta^{(b)}$ denotes residuals at the downsampling blocks and $\Delta^{(\text{mid})}$ the mid-block residual [17]. Before injecting these residuals into the main denoising U-Net, we apply a FiLM-style feature-wise affine gate [18] to regulate residual strength. This can be expressed as,

$$\begin{aligned} \tilde{\Delta}^{(b)} &= \gamma^{(b)} \odot \Delta^{(b)} + \beta^{(b)}, \\ \tilde{\Delta}^{(\text{mid})} &= \gamma^{(\text{mid})} \odot \Delta^{(\text{mid})} + \beta^{(\text{mid})}, \end{aligned} \quad (8)$$

where (γ, β) are learnable scale and bias parameters and \odot represents element wise multiplication.

d) *Training objective*: Stage B is trained with the standard noise-prediction objective used in DDPM/LDMs [8, 9]. For each training iteration, the denoiser predicts

$$\hat{\epsilon} = \epsilon_\theta(z_t, t, c_{\text{text}}; \{\tilde{\Delta}^{(b)}\}, \tilde{\Delta}^{(\text{mid})}), \quad (9)$$

and we minimize the mean-squared error to the injected noise,

$$\mathcal{L}_B = \mathbb{E}_{I \sim \mathcal{D}, t, \epsilon} \left[\|\epsilon - \hat{\epsilon}\|_2^2 \right]. \quad (10)$$

C. Inference

As given in the figure 4, at the inference, we first sample a semantic layout using Stage A. From the input prompt, we extract the domain label d and the user-specified ratio targets r and form the conditioning embedding e . The discrete reverse chain is initialized from categorical noise z_{T_1} and run for T_1 steps. At each step, the U-Net predicts logits ℓ_θ , which parameterize the reverse transition distribution $p_\theta(x_{t-1} | x_t, e)$, and we sample $x_{t-1} \sim p_\theta(x_{t-1} | x_t, e)$. After the final step, we obtain the generated one-hot layout \hat{x}_0 , which is upsampled to the conditioning resolution required by Stage B.

Stage B then synthesizes an image conditioned on the generated layout and the same prompt. We initialize the latent from Gaussian noise $z_{T_2} \sim \mathcal{N}(0, \mathbf{I})$ and iteratively denoise for T_2 steps using a latent diffusion sampler, conditioned on (i) the CLIP prompt embeddings c_{text} and (ii) the upsampled layout \hat{x}_0 provided to ControlNet for spatial guidance. The final latent is decoded by the VAE decoder to obtain the synthetic satellite image \hat{I} .

TABLE I: Combined downstream segmentation results with Original vs. Original+Synthetic training. Colors/bold indicate the gain of Original+Synthetic over the corresponding Original value for each cell: **red** ($\geq +10$), **blue** (+5 to +10), **bold** (0 to +5).

| Model | Training Dataset | IoU (%) | | | | | | | mIoU | mF1 | OA |
|---|------------------|--------------|--------------|--------------|--------------|--------------|--------------|--------------|--------------|--------------|--------------|
| | | Background | Building | Road | Water | Barren | Forest | Agriculture | | | |
| (A) In-domain evaluation | | | | | | | | | | | |
| U-Net [21] | Orig. | 45.91 | 53.74 | 45.27 | 58.10 | 17.13 | 35.13 | 23.11 | 39.77 | 58.22 | 55.35 |
| | Orig.+Syn. | 54.79 | 63.10 | 52.68 | 68.66 | 27.43 | 40.20 | 52.64 | 51.36 | 70.24 | 66.85 |
| PSPNet [22] | Orig. | 51.31 | 57.23 | 41.14 | 50.45 | 19.22 | 36.27 | 45.45 | 43.01 | 64.20 | 59.14 |
| | Orig.+Syn. | 52.53 | 61.95 | 48.76 | 59.54 | 21.41 | 40.00 | 47.93 | 47.45 | 67.11 | 63.26 |
| FactSeg [23] | Orig. | 50.66 | 55.09 | 48.67 | 63.40 | 26.28 | 36.75 | 41.22 | 46.01 | 64.83 | 62.16 |
| | Orig.+Syn. | 52.79 | 62.40 | 53.03 | 66.96 | 24.80 | 42.98 | 46.71 | 49.95 | 65.57 | 68.11 |
| HRNet [24] | Orig. | 50.31 | 59.15 | 45.53 | 62.97 | 31.08 | 39.71 | 43.21 | 47.43 | 65.55 | 63.68 |
| | Orig.+Syn. | 55.44 | 61.21 | 55.77 | 71.99 | 29.04 | 38.14 | 59.49 | 53.01 | 71.87 | 68.20 |
| AerialFormer [25] | Orig. | 54.40 | 66.09 | 56.04 | 69.44 | 28.99 | 45.48 | 50.96 | 53.06 | 68.40 | 65.57 |
| | Orig.+Syn. | 55.26 | 67.55 | 56.23 | 67.13 | 32.50 | 45.92 | 55.21 | 54.26 | 69.61 | 68.35 |
| (B) Domain generalization | | | | | | | | | | | |
| Urban \rightarrow Rural | | | | | | | | | | | |
| FactSeg [23] | Orig. | 53.10 | 41.24 | 29.58 | 22.80 | 12.60 | 10.80 | 42.38 | 30.36 | 44.55 | 61.44 |
| | Orig.+Syn. | 53.68 | 42.95 | 34.97 | 33.81 | 12.72 | 22.19 | 48.35 | 35.52 | 50.87 | 63.48 |
| HRNet [24] | Orig. | 51.09 | 46.50 | 27.07 | 25.57 | 15.45 | 8.06 | 27.99 | 28.82 | 42.84 | 57.29 |
| | Orig.+Syn. | 55.25 | 45.20 | 35.42 | 37.11 | 16.56 | 8.40 | 45.45 | 34.77 | 49.04 | 64.20 |
| Rural \rightarrow Urban | | | | | | | | | | | |
| FactSeg [23] | Orig. | 36.92 | 42.54 | 18.88 | 61.36 | 34.72 | 38.85 | 46.59 | 39.98 | 56.07 | 58.38 |
| | Orig.+Syn. | 39.07 | 57.00 | 49.17 | 63.86 | 42.25 | 52.14 | 49.65 | 50.45 | 66.71 | 65.16 |
| HRNet [24] | Orig. | 38.78 | 41.31 | 30.24 | 68.65 | 39.29 | 42.95 | 46.43 | 43.95 | 60.30 | 60.51 |
| | Orig.+Syn. | 40.54 | 58.17 | 50.63 | 70.69 | 46.04 | 53.46 | 57.02 | 53.79 | 69.52 | 68.53 |

D. Synthetic Dataset Construction and Downstream Segmentation

Starting from running pixel-frequency statistics over real and accepted synthetic masks, we use a greedy enrichment strategy that repeatedly selects the most underrepresented non-background class in each domain and proposes ratio constraints to upweight it. Candidate layouts are accepted only if realized ratios satisfy the domain-specific constraints within a tolerance. We created 894 Rural and 1106 Urban additional samples (altogether 2000 pairs of images and labels), which are mixed with the original LoveDA training split. We then train five representative segmentation models, U-Net [21], PSPNet [22], FactSeg [23], HRNet [24], and AerialFormer [25], using an identical recipe on (i) real-only and (ii) real+synthetic data, and evaluate on the official LoveDA validation split. Results are reported in terms of mIoU and per-class IoU, emphasizing minority-class gains and cross-domain robustness.

III. RESULTS AND DISCUSSION

Figure 1 shows that the original LoveDA split is strongly long-tailed and domain-dependent, with minority categories receiving very limited pixel supervision. The mixed distribution has a higher exposure to minority classes without breaking domain realism, consistent with the controlled examples in Figure 1(b–f).

Table I shows that adding ratio-controlled synthetic pairs consistently improves segmentation across backbones, with

the largest gains concentrated on minority and mid-tail classes rather than only the head classes. In-domain, mIoU increases for all models, with particularly strong improvements in agriculture, road, and water, indicating that synthesis mainly contributes context diversity for underrepresented semantics while respecting Urban/Rural style constraints. In domain generalization, synthesis has also improved transfer in both directions, suggesting reduced reliance on source-domain co-occurrence shortcuts.

IV. CONCLUSION

We proposed a prompt-controlled diffusion-based data augmentation framework for LoveDA that explicitly addresses the coupled challenges of long-tailed pixel imbalance and Urban/Rural domain shift. By conditioning generation on domain identity and class-ratio targets, our approach enables targeted synthesis of samples that increase effective exposure to underrepresented classes while preserving domain-consistent remote-sensing realism. Experiments show that augmenting the original training set with greedily generated Urban and Rural samples consistently improves segmentation performance, particularly for minority classes, and reduces the domain gap across backbones. While ratio adherence degrades for extrapolative targets far from learned co-occurrence statistics and evaluation is currently limited to LoveDA, the results demonstrate that controllable generative augmentation is a practical and effective tool for mitigating long-tail imbalance in remote-sensing segmentation.

REFERENCES

[1] Q. Yuan, H. Shen, T. Li, Z. Li, S. Li, Y. Jiang, H. Xu, W. Tan, Q. Yang, J. Wang, J. Gao, and L. Zhang, “Deep learning in environmental remote sensing: Achievements and challenges,” *Remote Sensing of Environment*, vol. 241, p. 111716, 2020.

[2] L. Ma, Y. Liu, X. Zhang, Y. Ye, G. Yin, and B. A. Johnson, “Deep learning in remote sensing applications: A meta-analysis and review,” *ISPRS Journal of Photogrammetry and Remote Sensing*, vol. 152, pp. 166–177, 2019.

[3] J. Wang, Z. Zheng, A. Ma, X. Lu, and Y. Zhong, “Loveda: A remote sensing land-cover dataset for domain adaptive semantic segmentation,” in *Proceedings of the IEEE/CVF International Conference on Computer Vision (ICCV)*, 2021.

[4] Y. Cui, M. Jia, T.-Y. Lin, Y. Song, and S. Belongie, “Class-balanced loss based on effective number of samples,” in *2019 IEEE/CVF Conference on Computer Vision and Pattern Recognition (CVPR)*, 2019, pp. 9260–9269.

[5] T.-Y. Lin, P. Goyal, R. Girshick, K. He, and P. Dollár, “Focal loss for dense object detection,” in *2017 IEEE International Conference on Computer Vision (ICCV)*, 2017, pp. 2999–3007.

[6] A. Shrivastava, A. Gupta, and R. Girshick, “Training region-based object detectors with online hard example mining,” in *Proceedings of the IEEE Conference on Computer Vision and Pattern Recognition (CVPR)*, 2016, pp. 761–769.

[7] E. D. Cubuk, B. Zoph, D. Mane, V. Vasudevan, and Q. V. Le, “Autoaugment: Learning augmentation strategies from data,” in *Proceedings of the IEEE/CVF Conference on Computer Vision and Pattern Recognition (CVPR)*, 2019.

[8] J. Ho, A. Jain, and P. Abbeel, “Denoising diffusion probabilistic models,” *arXiv preprint arXiv:2006.11239*, 2020. [Online]. Available: <https://arxiv.org/abs/2006.11239>

[9] R. Rombach, A. Blattmann, D. Lorenz, P. Esser, and B. Ommer, “High-resolution image synthesis with latent diffusion models,” in *Proceedings of the IEEE/CVF Conference on Computer Vision and Pattern Recognition (CVPR)*, 2022, pp. 10674–10685.

[10] A. Sebaq and M. ElHelw, “Rsdiff: Remote sensing image generation from text using diffusion model,” *Neural Computing and Applications*, vol. 36, no. 36, pp. 23 103–23 111, 2024. [Online]. Available: <http://dx.doi.org/10.1007/s00521-024-10363-3>

[11] O. Baghirlili, H. Askarov, I. Ibrahimli, I. Bakhishov, and N. Nabiyev, “Satdm: Synthesizing realistic satellite image with semantic layout conditioning using diffusion models,” *arXiv preprint arXiv:2309.16812*, 2023. [Online]. Available: <https://arxiv.org/abs/2309.16812>

[12] B. Kim, M. Bae, and J.-G. Lee, “Sample-efficient multi-round generative data augmentation for long-tail instance segmentation,” in *Advances in Neural Information Processing Systems (NeurIPS)*, 2025.

[13] J. Niemeijer, J. Ehrhardt, H. Handels, and H. Uzunova, “Uncertainty-aware controlnet: Bridging domain gaps with synthetic image generation,” *arXiv preprint arXiv:2510.11346*, 2025. [Online]. Available: <https://arxiv.org/abs/2510.11346>

[14] R. Yu, S. Liu, X. Yang, and X. Wang, “Distribution shift inversion for out-of-distribution prediction,” *arXiv preprint arXiv:2306.08328*, 2023. [Online]. Available: <https://arxiv.org/abs/2306.08328>

[15] Y. Qin, H. Zheng, J. Yao, M. Zhou, and Y. Zhang, “Class-balancing diffusion models,” *arXiv preprint arXiv:2305.00562*, 2023. [Online]. Available: <https://arxiv.org/abs/2305.00562>

[16] J. Austin, D. D. Johnson, J. Ho, D. Tarlow, and R. van den Berg, “Structured denoising diffusion models in discrete state-spaces,” *CoRR*, vol. abs/2107.03006, 2021.

[17] L. Zhang, A. Rao, and M. Agrawala, “Adding conditional control to text-to-image diffusion models,” in *Proceedings of the IEEE/CVF International Conference on Computer Vision (ICCV)*, 2023.

[18] E. Perez, F. Strub, H. de Vries, V. Dumoulin, and A. Courville, “Film: Visual reasoning with a general conditioning layer,” in *Proceedings of the AAAI Conference on Artificial Intelligence*, 2018.

[19] A. Radford, J. W. Kim, C. Hallacy, A. Ramesh, G. Goh, S. Agarwal, G. Sastry, A. Askell, P. Mishkin, J. Clark, G. Krueger, and I. Sutskever, “Learning transferable visual models from natural language supervision,” *arXiv preprint arXiv:2103.00020*, 2021. [Online]. Available: <https://arxiv.org/abs/2103.00020>

[20] T. Park, M.-Y. Liu, T.-C. Wang, and J.-Y. Zhu, “Semantic image synthesis with spatially-adaptive normalization,” in *Proceedings of the IEEE/CVF Conference on Computer Vision and Pattern Recognition (CVPR)*, 2019, pp. 2332–2341.

[21] O. Ronneberger, P. Fischer, and T. Brox, “U-net: Convolutional networks for biomedical image segmentation,” in *Medical Image Computing and Computer-Assisted Intervention (MICCAI)*, 2015, pp. 234–241.

[22] H. Zhao, J. Shi, X. Qi, X. Wang, and J. Jia, “Pyramid scene parsing network,” in *2017 IEEE Conference on Computer Vision and Pattern Recognition (CVPR)*, 2017, pp. 6230–6239.

[23] A. Ma, J. Wang, Y. Zhong, and Z. Zheng, “Factseg: Foreground activation-driven small object semantic segmentation in large-scale remote sensing imagery,” *IEEE Transactions on Geoscience and Remote Sensing*, vol. 60, pp. 1–16, 2022.

[24] J. Wang, K. Sun, T. Cheng, B. Jiang, C. Deng, Y. Zhao, D. Liu, Y. Mu, M. Tan, X. Wang, W. Liu, and B. Xiao, “Deep high-resolution representation learning for visual recognition,” *IEEE Transactions on Pattern Analysis and Machine Intelligence*, vol. 43, no. 10, pp. 3349–3364, 2021.

[25] T. Hanyu, K. Yamazaki, M. Tran, R. A. McCann, H. Liao, C. Rainwater, M. Adkins, J. Cothren, and N. Le, “Aerialformer: Multi-resolution transformer for aerial image segmentation,” *Remote Sensing*, vol. 16, no. 16, p. 2930, 2024.